arXiv:1402.7145v1 [cond-mat.mes-hall] 28 Feb 2014

Dispersion of Fermi arcs in Weyl semimetals and their evolutions to Dirac cones

Ryo Okugawa[1] and Shuichi Murakami[1,2]

[1] *Department of Physics, Tokyo Institute of Technology, 2-12-1 Ookayama, Meguro-ku, Tokyo 152-8551, Japan*

[2] *TIES, Tokyo Institute of Technology, 2-12-1 Ookayama, Meguro-ku, Tokyo 152-8551, Japan*

(Dated: March 3, 2014)

We study dispersions of Fermi arcs in the Weyl semimetal phase by constructing a simple effective model. We calculate how the surface Fermi-arc dispersions for top- and bottom surfaces merge into the bulk Dirac cones in the Weyl semimetal at both ends of the arcs, and show that they have opposite velocities. This result is also confirmed by a calculation using a tight-binding model. Furthermore, by changing a parameter in the system while preserving time-reversal symmetry, we show that two Fermi arcs evolve into a surface Dirac cone when the system transits from the Weyl semimetal to the topological insulator phase. We also demonstrate that choices of surface terminations affect the pairing of Weyl nodes, from which the Fermi arcs are formed.

PACS numbers: 73.20.At, 73.43.Nq, 72.25.Dc

I. INTRODUCTION

Topological classification of phases has been one of the fruitful ways to explore new quantum phases in condensed materials. A topological insulator (TI) is one of the topological phases in condensed materials with time-reversal (TR) symmetry[1,2]. As a manifestation of topological properties of three-dimensional TIs, their band structure is gapped in the bulk, but is gapless in the surface. The surface states are determined by topological invariants calculated from the bulk states. The topological invariants are Z_2 topological numbers defined in TR invariant systems, and the resulting gapless surface states are protected topologically.

On the other hand, more recent works have revealed another kind of topological phases, not in insulators but in semimetals: for example, Weyl semimetals (WSs). In WSs, the conduction and valence bands form non-degenerate Dirac cones. They touch at isolated points in $\boldsymbol{k}$ space, called Weyl nodes. Remarkably, the Weyl nodes are stable topologically, because they are associated with a topological number called a monopole charge in $\boldsymbol{k}$ space, associated with the Berry curvature in $\boldsymbol{k}$ space. The topological WS phases are realized in 3D systems where TR or inversion (I) symmetry is broken. As candidates of the WSs with broken TR symmetry, pyrochlore iridates[3,4], multilayer structures consisting of TI with ferromagnetic order and normal insulator (NI)[5], and $HgCr_2Se_4$[6] are proposed. The multilayer structure of TI and NI with an external electric field is also suggested as a candidate material for the WS where I symmetry is broken.[7]

The number of Weyl nodes in 3D $\boldsymbol{k}$ space is necessarily even. It is because the Weyl nodes are either a monopole or an antimonopole in $\boldsymbol{k}$ space[8–10], and the sum of the monopole charge inside the Brillouin zone should vanish. Moreover, these Weyl nodes are robust topologically as long as translational symmetry is preserved.

Another remarkable topological property of WSs is an existence of topologically protected surface states[3]. The surface states form arcs in $\boldsymbol{k}$ space, which are called Fermi arcs, connecting between the Weyl nodes projected to the surface Brillouin zone. The appearance of Fermi arcs is explained in terms of a topological number when the Fermi energy is exactly on the Weyl nodes. As a result, the Fermi arc connects two Weyl nodes, one being a monopole and the other an antimonopole for the Berry curvature. On the other hand, the dispersion of the Weyl nodes is not well studied when the Fermi energy is away from the Weyl nodes. It is easily seen that the sign of the velocity of the Fermi-arc state is determined from the topological number, i.e. the monopole charge of the Weyl nodes, Moreover, as we find in this paper, the Fermi-arc dispersion has a unique form, which is useful to experimentally establish the WS phase. In this paper, we discuss surface state dispersion and bulk bands by constructing a simple effective model for the WS phase. The results from the effective model are confirmed by numerical calculations using a lattice model, which is the Fu-Kane-Mele model with an additional staggered on-site potential.

In the present paper, we focus on systems with TR symmetry and broken I symmetry. We also discuss phase transitions from the WS phase to other bulk insulating phases such as TI phases, and show changes of the surface energy band at the phase transitions by using a model realizing these phases. The I-symmetry breaking lifts the degeneracy of the surface states between the top surface and the bottom surface. When the system moves from WS to TI phases, we show that a pair of Fermi arcs evolves into a surface Dirac cone.

II. WEYL SEMIMETAL PHASE CHARACTERIZED BY THE BERRY CURVATURE

To characterize Weyl semimetals, Berry curvature in $\boldsymbol{k}$ space is important. As we explain below, the Weyl nodes are topological objects, corresponding to monopoles or

antimonopoles for the Berry curvature. This gives a strong restriction on behaviors of Weyl nodes. The Berry curvature in $\boldsymbol{k}$-space is introduced as follows.[8–10]. Let $\psi_\alpha(\boldsymbol{k})$ is the Bloch wavefunction and we write $\psi_\alpha(\boldsymbol{k}) = u_\alpha(\boldsymbol{k})e^{i\boldsymbol{k}\cdot\mathbf{r}}$, and $u_\alpha(\boldsymbol{k})$ is called a periodic part of the Bloch wavefunction. For the α-th band, the Berry connection (gauge field) $\boldsymbol{A}_\alpha(\boldsymbol{k})$ and the corresponding Berry curvature (field strength) $\boldsymbol{B}_\alpha(\boldsymbol{k})$ are defined as

$$\boldsymbol{A}_\alpha(\boldsymbol{k}) = i\langle u_\alpha(\boldsymbol{k})|\nabla_{\boldsymbol{k}}|u_\alpha(\boldsymbol{k})\rangle, \tag{1}$$
$$\boldsymbol{B}_\alpha(\boldsymbol{k}) = \nabla_{\boldsymbol{k}} \times \boldsymbol{A}_\alpha(\boldsymbol{k}), \tag{2}$$

and the corresponding monopole density is defined as

$$\rho_\alpha(\boldsymbol{k}) = \frac{1}{2\pi}\nabla_{\boldsymbol{k}} \cdot \boldsymbol{B}_\alpha(\boldsymbol{k}). \tag{3}$$

Properties of the monopole density is well studied[8–10]. Therefore we briefly outline its properties here. When the α-th band is not degenerate with other bands at some $\boldsymbol{k}$, the monopole density $\rho_\alpha(\boldsymbol{k})$ vanishes identically, because $u_\alpha(\boldsymbol{k})$ is analytic in the neighborhood of $\boldsymbol{k}$. Only at the $\boldsymbol{k}$-points where the α-th band touches with another band, the monopole density can be nonzero, having a δ-function singularity. It is shown from an argument on a gauge degree of freedom that the coefficient of δ-function is always an integer, and the monopole density has the form $\rho(\boldsymbol{k}) = \sum_l q_l \delta(\boldsymbol{k} - \boldsymbol{k}_l)$, where q_l is an integer. We call the integer q_l a monopole charge. In the simplest case of $q_l = \pm 1$ is called a monopole ($q_l = 1$) and an antimonopole ($q_l = -1$). The Weyl nodes are either a monopoles or an antimonopole, as one can see easily from an example Hamiltonian $H = \boldsymbol{k} \cdot \boldsymbol{\sigma}$, where $\boldsymbol{\sigma} = (\sigma_x, \sigma_y, \sigma_z)$ are the Pauli matrices. Because the monopole charge is quantized, the monopole charge cannot change under a continuous change of the Hamiltonian. They can only change at pair creation or pair annhilation of a monopole-antimonopole pair.

Time-reversal and inversion symmetries respectively give a restriction to these Berry curvature and monople density. The time-reversal symmetry leads to

$$\boldsymbol{B}_\alpha(\boldsymbol{k}) = -\boldsymbol{B}_{\alpha_R}(-\boldsymbol{k}),\ \rho_\alpha(\boldsymbol{k}) = \rho_{\alpha_R}(-\boldsymbol{k}), \tag{4}$$

where α_R is the band index obtained by time-reversal from αth band. Hence in time-reversal-symmetric systems, monopoles are distributed symmetrically with respect to the origin $\boldsymbol{k} = 0$. On the other hand, the inversion symmetry leads to

$$\boldsymbol{B}_\alpha(\boldsymbol{k}) = \boldsymbol{B}_{\alpha_I}(-\boldsymbol{k}),\ \rho_\alpha(\boldsymbol{k}) = -\rho_{\alpha_I}(-\boldsymbol{k}), \tag{5}$$

where α_I is the band index obtained by inversion from αth band. Hence in inversion-symmetric systems, monopoles are distributed antisymmetrically with respect to the origin $\boldsymbol{k} = 0$. Furthermore, in systems with both time-reversal and inversion symmetries, all states are doubly degenerate by Kramers theorem, and therefore a Dirac cone without degeneracy is impossible. Therefore, the Weyl semimetal requires either breaking of time-reversal symmetry or that of inversion symmetry, as has been proposed[5,7]. Such systems with broken time-reversal or inversion symmetries can be realized as multilayers of TIs and NIs[5,7,11].

III. EFFECTIVE MODEL FOR THE NI-SW-TI PHASE TRANSITION

To describe a Weyl semimetal and its evolution under a change of Hamiltonian parameters, we construct a minimal model including only a single valence band and a single conduction band. Therefore, we consider a minimal model described by a 2×2 matrix $H(\boldsymbol{k}, m)$, where m is introduced as a control parameter for NI-WS-TI phase transition. The 2×2 Hamiltonian $H(\boldsymbol{k}, m)$ is expanded as

$$H(\boldsymbol{k}, m) = a_0(\boldsymbol{k}, m) + \sum_{i=1}^{3} a_i(\boldsymbol{k}, m)\sigma_i, \tag{6}$$

where σ_i $(i = 1, 2, 3)$ are the Pauli matrices. The gap between the two eigenvalues closes when the three conditions

$$a_i(\boldsymbol{k}, m) = 0 \quad (i = 1, 2, 3) \tag{7}$$

are satisfied. If Eq. (7) has solutions for $\boldsymbol{k}$ at a given value of m, the bands generally form a Dirac cone without degeneracy at these $\boldsymbol{k}$ points, if $\frac{\partial(a_1,a_2,a_3)}{\partial(k_x,k_y,k_z)} \neq 0$. Therefore it is generally a Weyl semimetal, and the respective Weyl nodes are monopoles or antimonopoles, depending on the monopole charge equal to $\mathrm{sgn}\frac{\partial(a_1,a_2,a_3)}{\partial(k_x,k_y,k_z)} = \pm 1$.

Let us then change the parameter m. In order to open a gap in the system, all the monopoles and antimonopoles should disappear via monopole-antimonopole pair annihilation. Conversely, if we begin with a system with a bulk gap at some parameter m, and if a change of m induces appearance of Weyl nodes, then it should involve monopole-antimonopole pair creation. One of the purposes of the present paper is to create a simple effective model describing the Weyl semimetal phase close to monopole-antimonopole pair creation or annihilation, i.e. near the phase transition between the WS phase and a bulk insulating phase. Let $m = m_0$ be the value of m where this monopole-antimonopole pair creation occurs. A part of the formalism here follows the previous paper by one of the authors[12].

Suppose we change the value of m through the phase transition between the WS phase and a phase with a bulk gap. It is accompanied by a pair creation or annihilation, and let m_0 denote the value of m where the phase transition occurs. Then on one side of m, e.g. $m < m_0$ the system is a WS with an monopole and antimonopole, while on the other side of m, e.g. $m > m_0$ the system is an insulator in the bulk, which can be a NI or a TI. At $m = m_0$ the gap closes at some point where the pair creation occurs, and let $\boldsymbol{k} = \boldsymbol{k}_0$ denote the point; namely,

it satisfies $\boldsymbol{a}(\boldsymbol{k}_0, m_0) = 0$. We expand the coefficients of Eq. (6) to the linear order around $\boldsymbol{k}_0$ and m_0:

$$\boldsymbol{a}(\boldsymbol{k}, m) = M\Delta\boldsymbol{k} + \Delta m\boldsymbol{N}, \tag{8}$$

where $\Delta k_j = k_j - k_{0j}$, $\Delta m = m - m_0$, and $M_{ij} = \frac{\partial a_i}{\partial k_j}\Big|_0$ and $N_i = \frac{\partial a_i}{\partial m}\big|_0$ are the values of derivatives at $m = m_0$ and $\boldsymbol{k} = \boldsymbol{k}_0$. It gives a generic Hamiltonian describing a pair creation of monopoles at $m = m_0$, shown in Ref. 12. From this Hamiltonian we can calculate the motion of the Weyl nodes close to the pair creation (i.e. the phase transition between the WS and the bulk insulating phase), and band dispersions[12].

It is also noted in Ref. 12 that pair creations occur in pairs at $\boldsymbol{k} = \boldsymbol{k}_0$ and $\boldsymbol{k} = -\boldsymbol{k}_0$ simultaneously, imposed by Eq. (4). Thus there are at least two monopoles and two antimonopoles in the WS with time-reversal symmetry (but without inversion symmetry). If one varies m further and the system becomes a bulk insulating phase again, there should be pair annihilations to make all the monopoles and antimonopoles disappear. If pair annihilations occur by exchanging partners from the pair creations, some of the four Z_2 topological numbers of 3D TIs should be different between the initial bulk-insulating phase and the final bulk-insulating phase.

Our goal here is to calculate an evolution of surface states through this change of the WS phase. To this goal the generic Hamiltonian described above is not convenient because it contains many parameters. Therefore, instead of using the above generic Hamiltonian, we use a simplified Hamiltonian. This is obtained from the above Hamiltonian after some gauge transformation, scale transformation, and a few simplifying assumptions. The details of this derivation is in Appendix A. The resulting effective model is described by a Hamiltonian

$$H = \gamma(k_x^2 - m)\sigma_x + v(k_y\sigma_y + k_z\sigma_z), \tag{9}$$

where v and γ are nonzero constants, and we choose them to be positive for simplicity. Its bulk dispersion is given by

$$E = \pm\sqrt{\gamma^2(k_x^2 - m)^2 + v^2k_y^2 + v^2k_z^2}. \tag{10}$$

The Fermi energy is assumed to be at $E = 0$. When $m < 0$ it describes a phase with a bulk gap $2\gamma|m|$, either the TI or the NI phase. On the other hand, when $m > 0$ the bulk gap closes at two points $\mathrm{W}_\pm$: $\boldsymbol{k} = (\pm\sqrt{m}, 0, 0)$. Around these points the dispersions are linear in three directions, and therefore it describes the WS phase. These two Weyl nodes W_+ and W_- are a monopole and an antimonopole for the lower band, respectively. At $m = 0$ there occurs a monopole-antimonopole pair creation.

Let us consider a surface of the WS phase with $m = m_0(> 0)$. Following the standard technique, we describe the surface by a space-dependent value of m. Namely, we regard m to change its sign at the surface. We set m to have a negative value in the vacuum side, and m converges to $m_0(> 0)$ in the WS side. The surface is assumed to be along the xy plane for simplicity. Therefore we set

$$\begin{cases} m(z) = m_0 & : \ z \to -\infty \\ m(z) < 0 & : \ z \to +\infty \end{cases} \tag{11}$$

for the surface normal to be $+\hat{z}$, which we call a top surface, and

$$\begin{cases} m(z) < 0 & : \ z \to -\infty \\ m(z) = m_0 & : \ z \to +\infty \end{cases} \tag{12}$$

for the surface normal to be $-\hat{z}$, which we call a bottom surface. They correspond to the top and bottom surfaces of a slab with sufficiently large thickness.

Here we calculate band dispersions for the top surface and for the bottom surface. By unitary transformation with $U = \frac{1}{\sqrt{2}}(1 - i\sigma_x)$, the Hamiltonian is transformed to

$$\begin{aligned} H' &\equiv U^{-1}HU = \gamma(k_x^2 - m)\sigma_x - iv\frac{\partial}{\partial z}k_z\sigma_y - vk_y\sigma_z \\ &= \begin{pmatrix} -vk_y & \gamma(k_x^2 - m) - v\frac{\partial}{\partial z} \\ \gamma(k_x^2 - m) + v\frac{\partial}{\partial z} & vk_y \end{pmatrix} \end{aligned} \tag{13}$$

Because we focus on the surface within the xy plane, we have replaced k_z with $-i\frac{\partial}{\partial z}$, while k_x and k_y are the Bloch wavenumbers. It is now straightforward to write down the eigenstates bound to the surfaces. The bound state on the top surface is given by

$$\psi_{\mathrm{T}} = \begin{pmatrix} 1 \\ 0 \end{pmatrix} e^{-(\gamma/v)\int^z (k_x^2 - m(z))dz}, \ E = -vk_y \tag{14}$$

and the bound state on the bottom surface is given by

$$\psi_{\mathrm{B}} = \begin{pmatrix} 0 \\ 1 \end{pmatrix} e^{(\gamma/v)\int^z (k_x^2 - m(z))dz}, \ E = vk_y \tag{15}$$

They are respectively allocated as top- and bottom-surface states, because otherwise the wavefunction diverges at some region and is not normalizable. We also note that both of these surface states exist only when

$$-\sqrt{m_0} < k_x < \sqrt{m_0}. \tag{16}$$

At $E = 0$, the surface states are degenerate, and are located at $k_y = 0, -\sqrt{m_0} < k_x < \sqrt{m_0}$, which is a line connecting the 2D projection of the Weyl points $\mathrm{W}_\pm$: $\boldsymbol{k} = (\pm\sqrt{m_0}, 0, 0)$. Thus these surface states are Fermi arcs. We note that the top-surface Fermi-arc states have a velocity $\boldsymbol{v} = \frac{\partial E}{\partial \boldsymbol{k}} = (0, -v)$ and those of the bottom-surface have a velocity $\boldsymbol{v} = \frac{\partial E}{\partial \boldsymbol{k}} = (0, v)$. Their signs are consistent with the fact that $\mathrm{W}_\pm$ are a monopole and an antimonopole, respectively. The signs follow from the fact that on the slice of the 3D BZ at $k_x = $ const. $(-\sqrt{m_0} < k_x < \sqrt{m_0})$ the lower band has a Chern number equal to -1.

We show how these surface states disperse if the Fermi energy is away from the Weyl point. To see how the bulk

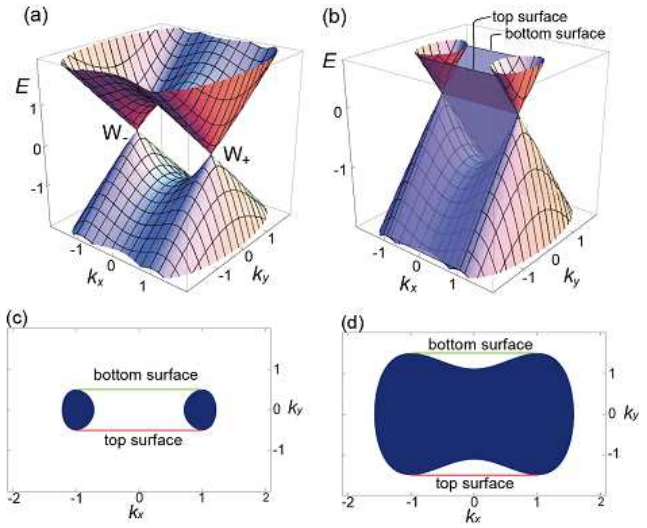

FIG. 1. Bulk and surface states of the model for the Weyl semimetal. The parameters are set as $v = \gamma = m_0 = 1$. (a) shows the bulk states, and (b) shows the surface Fermi arcs and the bulk states. (c)(d) The Fermi surface for the Fermi energy at (c) $E = 0.5$ and at (d) $E = 1.5$.

bands and surface bands are related, we project the bulk dispersion, Eq. (10), onto the surface. The resulting bulk bands are in regions

$$E > \sqrt{\gamma^2(k_x^2 - m_0)^2 + v^2 k_y^2}, \tag{17}$$

$$E < -\sqrt{\gamma^2(k_x^2 - m_0)^2 + v^2 k_y^2}, \tag{18}$$

which describe the conduction and the valence bands, respectively. These two bands touch each other at the projections of the two Weyl nodes $W_\pm$: $k_x = \pm\sqrt{m_0}$, $k_y = 0$. Around these Weyl nodes the dispersion is linear. This projected bulk band structure is shown in Fig. 1 (a), forming two Dirac cones around the Weyl nodes $W_\pm$. The surface states are tangential to these cones, as shown in Fig. 1 (b).

To see the relationship between the projection of the bulk bands and the surface states, we show the Fermi surface at a constant energy E. The bulk-band projection changes its topology at $E = \pm\gamma m_0$. When $-\gamma m_0 < E < \gamma m_0$, the bulk-band projection forms two distinct pockets as shown in Fig. 1 (c), and the Fermi arcs are bridged between these two pockets. When $|E| > \gamma m_0$, it forms one pocket with a dumb-bell-like structure (Fig. 1 (d)). In either case, it is remarkable that the Fermi arc merges to the bulk-band projection at the two ends, and at both ends they are tangential to the bulk-band projection.

IV. NUMERICAL CALCULATION OF SURFACE STATES OF WEYL SEMIMETALS IN A LATTICE MODEL

A. Model

In this section, we numerically calculate surface states in a WS phase and compare the results to the discussions in Sec. III. For this purpose, we begin with the Fu-Kane-Mele (FKM) tight-binding model[13], which is known to show various 3D TI phases. It does not show the WS phase as it is, because it does not break I symmetry. By adding a staggered on-site potential to the model to break I symmetry, it does show the WS phase as shown in Ref. 12. It was later used also in Ref. 14 to calculate surface Fermi arcs in some parameter range.

Hence, we use the FKM model with a staggered on-site potential added. Our model is a 3D tight-binding model on a diamond lattice, described by the following Hamiltonian

$$H = \sum_{\langle i,j\rangle} t_{ij} c_i^\dagger c_j + i\frac{8\lambda_{so}}{a^2} \sum_{\langle\langle i,j\rangle\rangle} c_i^\dagger \boldsymbol{s}\cdot(\boldsymbol{d}_{ij}^1 \times \boldsymbol{d}_{ij}^2) c_j + \lambda_v \sum_i \xi_i c_i^\dagger c_i, \tag{19}$$

where $\boldsymbol{s}$ are Pauli matrices and a is the lattice constant for the cubic unit cell. The first term is the nearest-neighbor hopping with hopping amplitude t_{ij}. The second term represents the spin-orbit interaction for next nearest neighbor hopping with a spin-orbit coupling parameter λ_{so}. $\boldsymbol{d}_{ij}^1$ and $\boldsymbol{d}_{ij}^2$ are the nearest neighbor vectors connecting second-neighbor sites i and j. The third term represents the staggered on-site energy $\pm\lambda_v$, where λ_v is a constant and $\xi_i = \pm 1$ depends on the sublattices, i.e. $\xi = +1$ for the A sublattice and $\xi = -1$ for B sublattice for the diamond lattice.

The model without the third term is the FKM model, and is TR and I symmetric[13]. Provided the nearest-neighbor hoppings t_{ij} are identical, the FKM model has gapless band structure with the bulk gap closed at the three X points, showing that it is a Dirac semimetal. There are four directions of the nearest neighbor bonds, and when the hopping integrals for four nearest-neighbor bonds t_α ($\alpha = 1, 2, 3, 4$) become different, the model shows various phases of either strong topological insulator (STI) or weak topological insulator (WTI) phases. The hopping integrals along the bond in the 111, $1\bar{1}\bar{1}$, $\bar{1}1\bar{1}$, and $\bar{1}\bar{1}1$ directions are denoted as t_1, t_2, t_3, and t_4, respectively.

To realize the WS phase with TR symmetry, the system needs to be I-asymmetric. In Ref. 12, it is shown that with the λ_v term breaking the I-symmetry, this model shows the WS phase. The Hamiltonian matrix is

$$\mathcal{H}(\boldsymbol{k}) = \begin{pmatrix} \lambda_v \mathbf{1} + \sum_{i=1}^3 F_i s_i & f\mathbf{1} \\ f^*\mathbf{1} & -\lambda_v 1 - \sum_{i=1}^3 F_i s_i \end{pmatrix} \tag{20}$$

where

$$f = t_1 + t_2 e^{i\boldsymbol{k}\cdot\boldsymbol{a_2}} + t_3 e^{i\boldsymbol{k}\cdot\boldsymbol{a_3}} + t_4 e^{i\boldsymbol{k}\cdot\boldsymbol{a_1}}, \tag{21}$$

$$F_x = -4\lambda_{so} \sin\frac{a}{2}k_x \Big(\cos\frac{a}{2}k_y - \cos\frac{a}{2}k_z\Big), \tag{22}$$

and F_y and F_z are given by cyclic permutation of the subscripts x, y, and z in F_x. The primitive vectors of the fcc lattice are defined as $\boldsymbol{a}_1 = \frac{a}{2}(1,1,0)$, $\boldsymbol{a}_2 = \frac{a}{2}(0,1,1)$, $\boldsymbol{a}_3 = \frac{a}{2}(1,0,1)$. The energy eigenvalues are

$$E(\boldsymbol{k}) = \pm\sqrt{(\lambda_v \pm |\boldsymbol{F}|)^2 + |f|^2}, \tag{23}$$

where $\boldsymbol{F} = (F_x, F_y, F_z)$. Therefore, the spectrum is gapless when

$$\mathrm{Re}f = \mathrm{Im}f = 0, \quad \lambda_v = \pm|\boldsymbol{F}|. \tag{24}$$

In some parameter region, the three equations (24) for three parameters k_x, k_y, and k_z have solutions, showing the locations of the Weyl nodes. The bulk gap is then closed and the WS phase appears there.

B. Numerical calculation of surface states

In Ref. 12, phase diagrams of this model are studied and this model is shown to exhibit the STI, WTI, and WS phases by changing parameters. As an example, we assume $t_1 = t + \delta t_1$, $t_2 = t + \delta t_2$, $t_3 = t_4 = t$ and $\delta t_- = \delta t_1 - \delta t_2$ is fixed to be positive while $\delta t_+ = \delta t_1 + \delta t_2$ is varied. For the case with I symmetry, i.e. $\lambda_v = 0$, a band inversion at $X^x = \frac{2\pi}{a}(1,0,0)$ occurs at $\delta t_+ = 0$, accompanied by a phase transition between the STI phase with the Z_2 topological number 1;(111) ($\delta t_+ > 0$) and the WTI phase with the Z_2 topological number 0;$(1\bar{1}\bar{1})$ ($\delta t_+ < 0$)[13]. As a result, when the system is in the STI phase, a surface Dirac cone arises at the point $X^x = \frac{2\pi}{a}(1,0,0)$ projected onto the surface Brillouin zone, while in the WTI phases there is no surface Dirac cone at this point.

If one introduces an on-site staggered potential λ_v, the I symmetry is broken while the TR symmetry is preserved. Then the WS phase intervenes between the STI and the WTI phases, as shown in Fig. 2 (a) In the WS phase, there are four Weyl nodes around the X^x point, as found in Ref. 12. These four Weyl nodes move as the parameter $\delta t_+ = \delta t_1 + \delta t_2$ changes. Among these four Weyl nodes, two are monopoles and the other two are antimonopoles, which distribute symmetrically with respect to the X^x point. On the surface, two Fermi arcs will arise, connecting monopole-antimonopole pairs. For calculation we fix $\delta t_- = \delta t_1 - \delta t_2 = 0.1t$ and $\lambda_{so} = 0.1t$.

To see surface states, we numerically diagonalize Eq. (19) in a slab geometry with (111) surfaces. To show the surface states, we take the z axis to be the surface normal along [111], the x axis along the surface in the $\boldsymbol{a_3} - \boldsymbol{a_1}$ direction and the y axis to be perpendicular to the x and z axes. The top surface of the slab is composed of lattice sites in the sublattice A and the bottom surface is composed of lattice sites in the sublattice B. Because the point X^x is projected to the point $M_2 = \frac{2\pi}{b}(0, 1/\sqrt{3})$ in the hexagonal surface Brillouin zone, the Dirac cones and the Fermi arcs appear around the point M_2. Here $b = a/\sqrt{2}$ is the length of the primitive vectors of the slab.

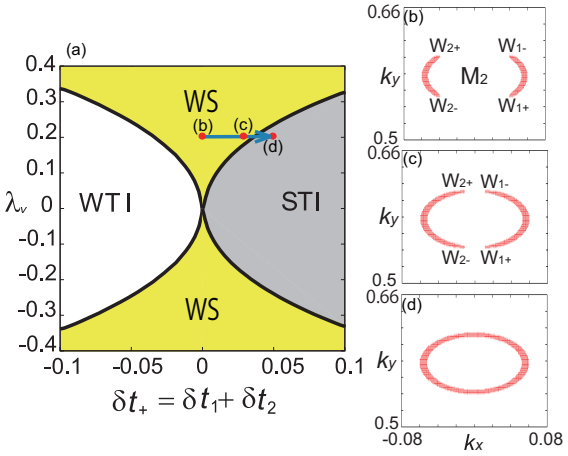

FIG. 2. (a) Phase diagram in the δt_+-λ_v plane, with $\delta t_- = 0.1t$ and $\lambda_{so} = 0.1t$, where $\delta t_\pm = \delta t_1 \pm \delta t_2$. The axes are in the unit of t. When $\lambda_v = 0$, the system is I-symmetric, and no WS phase appears. (b)(c)(d) Surface Fermi surface at $E = 0$ around the point M_2 near the Fermi level with $\lambda_v = 0.2t$ and the following values for δt_+: (b) $\delta t_+ = 0$ (WS), (c) $\delta t_+ = 0.03t$ (WS), and (d) $\delta t_+ = 0.05t$ (STI). The axes are in the unit of $2\pi/b$. (b) and (c) show Fermi arcs in the WS phase, and (d) shows a surface Dirac cone in the STI phase. We note that the end points of the surface Fermi arcs in the WS phase are the gapless points of the bulk bands.

Figure 2 (b)-(d) shows Fermi surfaces of a slab at $E = 0$ for various values of δt_+, with $\delta t_- = 0.1t$ and $\lambda_{so} = 0.1t$. For (b) $\delta t_+ = 0$ and (c) $\delta t_+ = 0.03$, the system is in the WS phase, and Fermi arcs appear around point M_2, corresponding to point X^x. The ends of arcs are the Weyl nodes projected into the surface Brillouin zone. Among the four Weyl points, let W_{1+} and W_{2+} denote the monopoles, and let W_{1-} and W_{2-} denote the antimonopoles, which are shown in Fig. 2 (b)(c). As δt_+ is changed, the Weyl nodes move around this M_2 points, and concomitantly the Fermi arcs grow as seen in Fig. 2(b) and (c). As δt_+ is increased further, the system eventually enters the STI phase. At the WS-STI phase transition, the Weyl nodes annihilate pairwise for (W_{1-},W_{2+}) and (W_{1+},W_{2-}), and there is no Weyl node in the STI phase, with a nonzero bulk gap. Correspondingly, as we see in Fig. 2(d), the two Fermi arcs in the WS phase are merged into a surface Dirac cone in the STI phase.

We discuss a relationship between the present work and the paper by Ojanen[14]. In the present work we fix the spin-orbit coupling λ_{so} to be a constant and change the anisotropy of the nearest neighbor hoppings. It enables

us to see the phase transitions from the WS phase to either the STI or the WTI phases. On the other hand, in Ojanen's paper[14] the spin-orbit parameter λ_{so} is changed across zero, to see the normal insulator (NI)-WS phase transitions. In approaching the WS-NI phase transition, the Fermi arcs are gradually shortened and eventually vanish.

So far we have discussed the surface states on $E = 0$, where the states on the top surface and those on the bottom surface are degenerate. The top-surface states and bottom-surface states are expected to have different dispersions, as Fig. 1 (b) shows. Figure 3 shows the results for the dispersion of the Fermi arcs on the top- and bottom-surface states in the present model. We note that the signs of the velocities are opposite between the top- and bottom-surface states, and their signs are consistent with the monopole charges of $\mathrm{W}_{i\pm}$ $(i = 1, 2)$. As is consistent with the result of the effective model (Fig. 1 (b)), each of these surface Fermi arcs is bridged between two Dirac cones around the Weyl nodes. As δt_+ is increased and the system undergoes the phase transition from the WS phase into the STI phase, the two Fermi arcs merge into a single Dirac cone on the top surface, and the same occurs on the bottom surface. As a result there arises a top-surface Dirac cone and a bottom-surface Dirac cone, which are non-degenerate as shown schematically in Fig. 4(a). This splitting of the Dirac cones are natural, because of the breaking of the I-asymmetry due to the staggered on-site energy λ_v. In the present case, the topmost layer in the top (bottom) surface is A-sublattice (B-sublattice), and therefore the top-surface (bottom-surface) states have a larger (smaller) energy due to the staggered on-site energy λ_v.

The surface states in the whole BZ for $\delta t_+ = 0$ (WS) and $\delta t_+ = 0.05t$ (STI) when $\lambda_v = 0.2t$ are shown in Fig. 5 (a1) and (b1). In addition to the surface states around M_2, there are Dirac cones around M_1 and M_3. Nevertheless, they are intact at the WTI-WS-STI phase transition, because this phase transition is related with a band inversion at X_x, which is projected onto M_2 point.

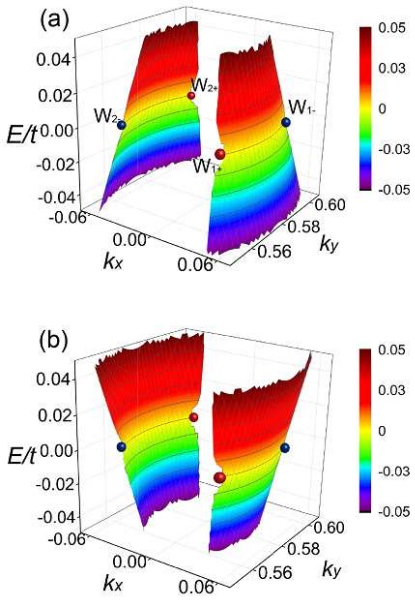

FIG. 3. Side views of the Fermi arcs around point $M_2 = \frac{2\pi}{b}(0, 1/\sqrt{3})$ with $\lambda_v = 0.2t$, $\delta t_+ = 0$ (WS phase). for (a) the top surface and (b) the bottom surface. The k_x and k_y axes are in the unit of $2\pi/b$. The red (blue) points are the gapless points which have positive (negative) monopole charges for the Berry curvature.

C. WS-TI phase transition and evolution of the Fermi-arc surface states

Based on the calculation results on the model (19), here we discuss general features of the evolution of the Fermi-arc surface states in the WS phase when some parameter is changed. In the WS phase there are an even number of Weyl nodes. In the I-asymmetric phases with TR symmetry, the minimal number is four, i.e. two monopoles and two antimonopoles, as follows from Eq. (4). In this case of two monopoles and antimonopoles, symmetrically distributed around a TRIM $\boldsymbol{k}_\Gamma$, the Fermi arcs are formed between monopole-antimonopole pairs, as exemplified in Fig. 2. Suppose then we change some parameter in the system. Due to topological nature of Weyl nodes, the monopoles and antimonopoles move in the 2D surface BZ. Eventually they may undergo some pair annihilations, which occur symmetrically with respect to the TRIM $\boldsymbol{k}_\Gamma$; the bulk bands become gapped. If a pair annihilation occurs for a pair connected by a Fermi arc, the Fermi arc eventually vanishes and the surface becomes gapped. On the other hand if the pair annihilation occurs between a monopole and an antimonopole, which are not connected to each other by the Fermi arc, the pair annihilations will make all the Fermi arcs into a single loop encircling the TRIM $\boldsymbol{k}_\Gamma$. This loop constitutes a Dirac cone around the TRIM.

From the viewpoint of the change of the Z_2 topological number and associated surface states, the evolution of the surface states accompanying the WTI-STI topological phase transition occurs in the following way. When the I-symmetry is broken, there should generally arise a WS phase between the WTI-STI phase transition. In the WTI-WS phase transition, two pairs of Weyl nodes are created close to a TRIM $\boldsymbol{k}_\Gamma$[10]. As the system enters the WS phase, a Fermi arc is formed between the two Weyl nodes within each pair. Thus there are two Fermi arcs which are symmetric with respect to the TRIM. As a control parameter is changed, the Fermi arcs grow as the Weyl nodes travel around the TRIM. Eventually, at the WS-STI phase transition, the four Weyl nodes annihilate pairwise, causing a fusion of two Fermi arcs into a single Dirac cone encircling the TRIM, as shown by Fig. 4 .

In Ref. 15 it is argued that when inversion symmetry is preserved, a Z_2 topological index defined for each surface TRIM indicates whether the focused surface TRIM is inside or outside the surface Fermi surface. It is also concluded that this index depends on the surface termination. Within this argument in Ref. 15, the surface should include the inversion center, and therefore there are two possible surface terminations for a fixed surface orientation. If we change one surface termination into the other, surface TRIM which were inside the Fermi surface will become outside the Fermi surface, and vice versa. We now try to apply this scenario to our model. However, the inversion symmetry is broken in our model, and the discussion in Ref. 15 is not directly applied, Nevertheless, we can expect the similar physics from continuity argument, by switching on the inversion-symmetry breaking. For example, in Fig. 5 (a1)(b1), we show the Fermi surface on the (111) surface with the surface terminated with the atoms, each of which has three bonds along $1\bar{1}\bar{1}$, $\bar{1}1\bar{1}$, and $\bar{1}\bar{1}1$. In this surface termination, the top surface is terminated by atoms in the A sublattice, and the bottom surface by atoms in the B sublattice. By adding bonds (i.e. "dangling bonds") along 111 directions to the topmost atoms, we can switch from one surface termination to the other, namely the top and the bottom surfaces terminated by B and A sublattices, respectively. The results are plotted in Fig. 5 (a2)(b2), whose parameters are identical with (a1) and (b1), respectively. We can see that the physics discussed in Ref. 15 carries over to the present model as well. For example, the M_1 and M_3 points are inside the Fermi surfaces when the dangling bonds are absent (Fig. 5(a1)(b1)), but when the dangling bonds are added, the Fermi surfaces around the M_1 and M_3 points disappear (Fig. 5(a2)(b2)). On the other hand, there appear a new Fermi surface around the Γ point when the dangling bonds are added. The remarkable phenomenon occurs around the M_2 point. The Fermi surface around the M_2 point in the STI phase in (b1) disappears in the plot (b2) where the dangling bonds are present. This also affects the neighboring WS phase, as can be seen by comparing (a1) and (a2). Among the Weyl nodes in (a1) the Fermi arcs arise between W_{1+}-W_{1-} and between W_{2+}-W_{2-}. Meanwhile in (a2), the Fermi arcs arise between W_{1+}-W_{2-} and between W_{2+}-W_{1-}. Thus we have shown that the change of surface termination exchanges the pairs of Weyl nodes, out of which the Fermi arcs are formed.

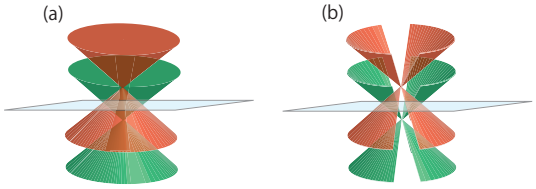

FIG. 4. Schematic drawing of the surface energy bands around a TRIM. The red (green) cone is the top (bottom) surface states. (a) In the STI phase, the two Dirac cones on the top and bottom surfaces are split in energy when the I symmetry is broken. (b) In the WS phase, there are a pair of Fermi arcs on each surface. These Fermi arcs will evolve into a Dirac cone shown in (a) in the STI phase.

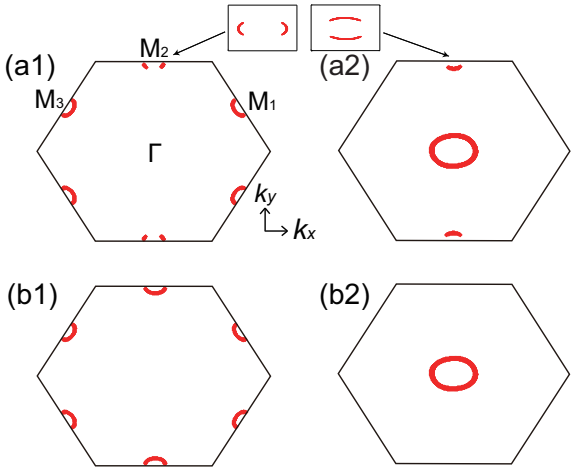

FIG. 5. The surface Fermi surfaces at $E = 0$ in the whole BZ when $\lambda_v = 0.2t$. The values of δt_+ is $\delta t_+ = 0$ (WS) for (a1) and (a2), and $\delta t_+ = 0.05t$ (STI) for (b1) and (b2). In (a1) and (b1), the surfaces are terminated without dangling bonds, and in (a2) and (b2) with dangling bonds. The insets show the magnified images of the surface Fermi surface around the M_2 point.

V. CONCLUSION

In the present paper, we study dispersions of Fermi arcs in the Weyl semimetal phase. We first construct a simple effective model, describing the Weyl semimetal with two Weyl nodes close to each other. We find that the dispersions of Fermi-arc states for top- and bottom surfaces cross around the Weyl point, and they have opposite velocities. These Fermi-arc dispersions are tangential to the bulk Dirac cones around the Weyl points. These results are confirmed by a calculation using a tight-binding model with time-reversal symmetry but without inversion symmetry. In this model calculation, we see that the Fermi arcs gradually grows by changing a model parameter, and that two Fermi arcs finally merge together to form a single Dirac cone when the system transits from the Weyl semimetal to the topological insulator phase. We also find that by changing the surface termination, the pairing between the two monopoles and two antimonopoles to make Fermi arcs are switched. These results reveals an interesting interplay between the surface and the bulk electronic states in Weyl semimetals and topological insulators.

ACKNOWLEDGMENTS

We are grateful to L. Balents for fruitful discussions. This research is supported in part by MEXT KAKENHI Grant Numbers 21000004, 22540327 and by the National Science Foundation under Grant No. NSF PHY11-25915 through Kavli Institute for Theoretical Physics, University of California at Santa Barbara, where part of the present work was completed.

Appendix A: Effective model close to monopole-antimonopole pair creation or annihilation in $\boldsymbol{k}$ space

From the Hamiltonian (6) with (8), one can derive an effective model describing the Weyl semimetal phase close to a monopole-antimonopole pair creation/annihilation. The argument closely follows that in Ref. 12. We note that Δm is a control parameter for Hamiltonian, and our goal is to construct the Hamiltonian where positive and negative Δm represents the WS and the bulk insulating phases, respectively. First we note that the determinant of the matrix M in (8) is zero, because otherwise the gapless condition (7) guarantees existence of $\boldsymbol{k}$ for both the positive and the negative values of Δm, meaning that both the positive and negative sides of Δm are conducting in the bulk. Hence we have $\det M = 0$, and therefore, the matrix M has a unit eigenvector $\boldsymbol{n}_1$ with zero eigenvalue: $M\boldsymbol{n}_1 = 0$. In Ref. 12, an orthonormal basis $\{\boldsymbol{n}_1, \boldsymbol{n}_2, \boldsymbol{n}_3\}$ is constructed out of this unit vector $\boldsymbol{n}_1$. While we can in principle proceed here as in Ref. 12, it leaves a number of free parameters in the model. In fact we can always set $\boldsymbol{n}_1 = {}^t(1,0,0)$, $\boldsymbol{n}_2 = {}^t(0,1,0)$, $\boldsymbol{n}_3 = {}^t(0,0,1)$, by a rotation of $\boldsymbol{k}$ coordinate axes. Then from (8) to the linear order in $\Delta\boldsymbol{k}$ and m, we have

$$\boldsymbol{a} = \Delta k_y \boldsymbol{u}_2 + \Delta k_z \boldsymbol{u}_3 + \Delta m \boldsymbol{N}, \tag{A1}$$

where $\boldsymbol{u}_i = M\boldsymbol{n}_i$ $(i = 2, 3)$. The gap closes when $\boldsymbol{a} = 0$, but it cannot happen in general for $\Delta m \neq 0$ because the three vectors $\boldsymbol{u}_2$, $\boldsymbol{u}_3$, $\boldsymbol{N}$ are generally linearly independent. It is an artifact of retaining only the linear terms in Δm and $\Delta\boldsymbol{k}$. Thus we have to include the next order in $\Delta\boldsymbol{k}$ and Δm. It turns out that the only relevant term here is the quadratic term in Δk_x[12] and therefore we additionally retain only this term, to obtain

$$\boldsymbol{a} = \Delta m \boldsymbol{N} + \Delta k_y \boldsymbol{u}_2 + \Delta k_z \boldsymbol{u}_3 + (\Delta k_x)^2 \boldsymbol{u}_{11}, \tag{A2}$$

where γ and v are positive constants. The gap closes when this vector is zero. The solution can be written down explicitly for generic cases, but instead we here introduce a simplifying assumption

$$\boldsymbol{u}_{11} = -\boldsymbol{N} = \begin{pmatrix} \gamma \\ 0 \\ 0 \end{pmatrix}, \ \boldsymbol{u}_2 = \begin{pmatrix} 0 \\ v \\ 0 \end{pmatrix}, \boldsymbol{u}_3 = \begin{pmatrix} 0 \\ 0 \\ v \end{pmatrix}. \tag{A3}$$

Namely, $\boldsymbol{u}_{11}$ and $\boldsymbol{N}$ are parallel, and they are orthogonal to $\boldsymbol{u}_2$ and $\boldsymbol{u}_3$. Then we get

$$\boldsymbol{a} = \begin{pmatrix} \gamma((\Delta p_1)^2 - m) \\ v\Delta p_2 \\ v\Delta p_3 \end{pmatrix}. \tag{A4}$$

It is straightforward to see that the solution for this exists only when m is positive. This means that positive m represents the WS phase while negative m means a bulk insulating phase. Within the WS phase, the Weyl nodes are given by $(\Delta k_x, \Delta k_y, \Delta k_z) = (\pm\sqrt{m}, 0, 0)$. If we have not employed the simplifying assumptions Eq. (A3), there arise terms in the expressions of the Weyl nodes, which are linear in m[12]. Nevertheless, these terms are not the main focus of the paper, and we discard them for simplicity for illustration of surface state dispersions and evolutions.

[1] C. L. Kane and E. J. Mele, Phys. Rev. Lett. **95**, 226801 (2005).
[2] B. A. Bernevig, T. L. Hughes, and S.-C. Zhang, Science **314**, 1757 (2006).
[3] X. Wan, A. M. Turner, A. Vishwanath, and S. Y. Savrasov, Phys. Rev. B **83**, 205101 (2011).
[4] K.-Y. Yang, Y.-M. Lu, and Y. Ran, Phys. Rev. B **84**, 075129 (2011).
[5] A. A. Burkov and L. Balents, Phys. Rev. Lett. **107**, 127205 (2011).
[6] G. Xu, H. Weng, Z. Wang, X. Dai, and Z. Fang, Phys. Rev. Lett. **107**, 186806 (2011).
[7] A. A. Burkov, M. D. Hook, and L. Balents, Phys. Rev. B **84**, 235126 (2011).
[8] M. V. Berry, Proc. Roy. Soc. London Ser A **392**, 45 (1984).
[9] G. E. Volovik and G. Volovik, *The universe in a helium droplet* (Oxford University Press, 2009).
[10] S. Murakami, New Journal of Physics **9**, 356 (2007).
[11] G. B. Halász and L. Balents, Phys. Rev. B **85**, 035103 (2012).
[12] S. Murakami and S. I. Kuga, Phys. Rev. B **78**, 165313 (2008).
[13] L. Fu, C. L. Kane, and E. J. Mele, Phys. Rev. Lett. **98**, 106803 (2007).
[14] T. Ojanen, Phys. Rev. B **87**, 245112 (2013).
[15] J. C. Y. Teo, L. Fu, and C. L. Kane, Phys. Rev. B **78**, 045426 (2008).